TITLE:

Turbulent Structures in Unsteady Open-Channel Flows

AUTHOR(S):

NEZU, Iehisa; NAKAGAWA, Hiroji; ISHIDA, Yoshihiro; KADOTA, Akihiro

CITATION:

NEZU, Iehisa ...[et al]. Turbulent Structures in Unsteady Open-Channel Flows. Memoirs of the Faculty of Engineering, Kyoto University 1995, 57(1): 1-25

ISSUE DATE:

1995-01-31

URL:

http://hdl.handle.net/2433/281499

RIGHT:

京都大学学術情報リポジトリ
KURENAI 紅
Kyoto University Research Information Repository

Turbulent Structures in Unsteady Open-Channel Flows

By

Iehisa NEZU, Hiroji Nakagawa, Yoshihiro Ishida and Akihiro Kadota*

(Received September 20, 1994)

Abstract

Turbulence measurements over a smooth wall in unsteady open-channel flows were conducted accurately by the simultaneous use of a two-component LDA system and water-wave gauges. The "general" log-law distributions, in which the von Karman constant is a universal one of $\kappa=0.41$ but the integration constant A is a function of main-flow conditions, were obeyed well in the wall region for both the rising and falling stages of flood. On the other hand, the log-wake law was reasonably applied to the outer region including the depth-varying zone. The Coles' wake parameter Π increased for the rising stage, whereas it decreased for the falling stage. The turbulence is stronger for the rising stage than for the falling stage, except for very near the free surface. These unsteady characteristics in open-channel flows with variation of the water surface are quite different from those in closed duct flows. Of particular significance is the findings counterclockwise loops of velocity and turbulence against the varying depth in unsteady open-channel flows.

1. Introduction

Intensive investigations on the statistical structure of turbulence and also on coherent structure such as bursts and sweeps in steady open-channel flows have been conducted in the last 20 years by making use of hydrogen-bubble techniques, hot-film anemometers and the laser-Doppler anemometer (LDA). The comprehensive knowledge on these topics is reviewed in the IAHR-monograph written by Nezu and Nakagawa [1]. Nezu *et al.* [2] have recently verified that the time-averaged data which were measured accurately with LDA in laboratory free-surface flumes can be applied to flow structures of actual rivers and estuaries at high Reynolds numbers, including the complex features of secondary currents and turbulence. This suggests strongly that such accurate laboratory data of open-channel flows are very contributory to hydraulic and river engineering in *steady* geophysical flows.

In contrast, rivers in flood are characterized by unsteadiness of flow. It is often

*Division of Civil and Global Environment Engineering Graduate School of Engineering Kyoto University, Kyoto 606, Japan

observed in rivers that the relation between the flow depth $h(t)$ and the discharge $Q(t)$ does not show a single curve, but a loop in the stronger *unsteady* flow; a peak discharge appears *before* a peak stage of the flow depth [3]. Significant differences of the flow and the associated sediment transport between the rising and falling stages of flood have been pointed out by many river engineers [4].

However, turbulent structures in *unsteady open-channel flows* have not been investigated as yet, because experimental equipment of unsteady free-surface flumes was not so elaborately constructed and also because turbulence measurements in water flows were much more difficult than those of *unsteady pipe flows and boundary layers* in a wind tunnel. For example, the latter information is available in a comprehensive review paper [5].

Hayashi *et al.*[6] have first conducted some turbulence measurements in unsteady free-surface flow by making use of hot-film anemometers; their unsteady water discharge was controlled by a mechanical valve. They suggested that turbulence might be stronger in the rising stage than in the falling one. Tu and Graf [7] have used three micro-propeller flow-meters to measure velocities over a gravel bed in unsteady open-channel flows. They found that the bed shear stress became considerably larger in the rising stage than in the falling one.

Nezu and Nakagawa [8] have made a new hydraulic circulation system of water discharge that was automatically controlled by a micro-computer. This system can reproduce any hydrograph of floods in *unsteady* free-surface flows. They have successfully conducted some accurate measurements of velocity components by making use of a two-component LDA system. No probe (without a laser light) in LDA is especially suitable to measure unsteady flows because its device never disturbs the flow. They found the loop properties of the h-Q curve and then examined some turbulence characteristics over dune beds in an unsteady free-surface flow.

Nezu et al. [9, 10] have measured the water-suface profiles and velocity distributions over smooth and Nikuradse-type rough beds, respectively, in unsteady open-channel flows, by the simultaneous use of an LDA system and wave-gauge instruments. The validity of "general" log-law distributions, in which the von Karman constant is a universal one of $\kappa=0.41$ but the integration constant A is a function of main-flow conditions, were examined for both the rising and falling stages of flood over smooth and rough beds. Next, Nezu et al. [11] have evaluated the bed shear stress from such general log-law distributions of mean velocities. These observed values of bed shear stress coincided reasonably with the theoretical ones calculated from the momentum equation of unsteady flow.

In the present study, statistical structures of mean velocity and turbulence were intensively investigated in the same unsteady free-surface flume system as has been

used by the authors. In particular, turbulence measurements near the water-surface zone of flood flow were first conducted successfully with an LDA system; such measurements have always been difficult by the use of conventional velocity instruments such as a hot-film anemometer [1].

The validity of general log-law and The van Driest damping function very near the wall was verified in the wall region for the rising and falling stages of flood. A systematic deviation from the general log-law was observed in the outer region and this deviation was expressed reasonably by the Coles' wake function. The turbulence intensities and Reynolds stress against the flood time were investigated in the whole flow depth of flood water flows. These distributions normalized by the corresponding friction velocity in time were described well by the semi-theoretical curves of Nezu for *steady* open-channel flows [1]. However, it was strongly suggested that the turbulence very near the free surface in *unsteady* open-channel flow may be much more different from that in *steady* open-channel flow.

2. Theory of Unsteady Open-Channel Flows

2.1 Basic Equations

The governing equations of 2-D unsteady open-channel flows are obtained from the Navier-Stokes equations, (e. g., *see* the IAHR-monograph [1] and Fig. 1), as follows:

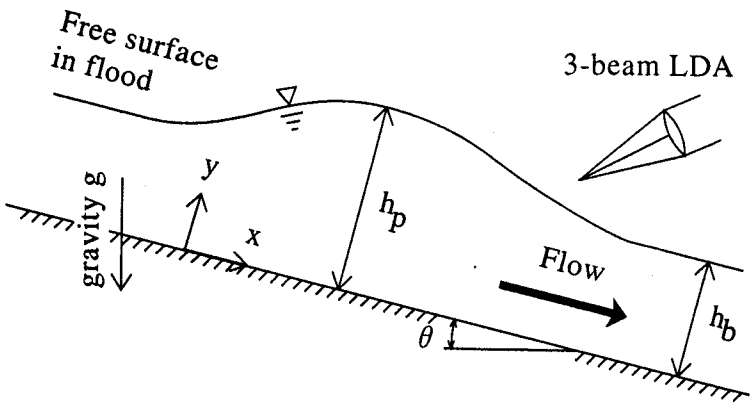

Fig. 1 Schematic description of unsteady free-surface flow. Even the depth-varying zone $h_b < y < h_p$ can be measured accurately with LDA.

$$\frac{\partial U}{\partial t}+\frac{\partial U^2}{\partial x}+\frac{\partial UV}{\partial y}=g\sin\theta-\frac{\partial P}{\rho\partial x}+\frac{\partial}{\partial y}\left(\frac{\tau}{\rho}\right) \tag{1}$$

$$0\cong-g\cos\theta-\frac{\partial P}{\rho\partial y}+\frac{\partial(-\overline{v^2})}{\partial y} \tag{2}$$

$$\text{where, } \frac{\tau}{\rho}\equiv-\overline{uv}+\nu\frac{\partial U}{\partial y} \tag{3}$$

U and V are the mean velocity components, and u and v the turbulence fluctuations in the streamwise (x) and vertical (y) directions, respectively. The mean pressure P is approximately given by the hydrostatic distribution using (2), as follows:

$$P=\rho g(h-y)\cos\theta \tag{4}$$

From (1) and (4), one can obtain

$$\frac{\partial U}{\partial t}+\frac{\partial U^2}{\partial x}+\frac{\partial UV}{\partial y}=gS_s+\frac{\partial}{\partial y}\left(\frac{\tau}{\rho}\right) \tag{5}$$

$$\text{where, } S_s\equiv\sin\theta-\cos\theta\frac{\partial h}{\partial x} \tag{6}$$

$S_b\equiv\sin\theta$ is the bed slope of channel, and h is the flow depth. Because $|\partial U/\partial t|\gg|\partial U^2/\partial x|$ and $|\partial UV/\partial y|$ in strong unsteady flow, the total shear stress τ can be obtained by integrating (5) from y to the free surface, i. e., $y=h$.

$$\frac{\tau}{\rho}\equiv-\overline{uv}+\nu\frac{\partial U}{\partial y}=gS_s(h-y)-\int_y^h\frac{\partial U}{\partial t}dy \tag{7}$$

$$\therefore\frac{\tau_b}{\rho}=gS_sh-\int_0^h\frac{\partial U}{\partial t}dy\cong gS_sR-\frac{1}{B}\frac{\partial Q}{\partial t} \tag{8}$$

The hydraulic radius R is adopted for the side-wall effects, and B is the channel width. Since the flow-depth gradient $\partial h/\partial x$ is approximately equal to $-(1/C)\partial h/\partial t$, the water-surface slope S_s is given by $S_b+(\cos\theta/C)\partial h/\partial t$. C is the celerity of flood waves and is given by $(gh)^{1/2}$ for long waves [3]. Therefore, S_s is larger in the rising stage of floods, whereas it is smaller in the falling stage. Nezu et al. [12] have recently found that the contribution of momentum gradient $|\partial U^2/\partial x|$ to the shear stress τ is negligibly small even in moderate unsteadiness.

2.2 Unsteadiness Parameter

It is necessary to reasonably define overall unsteadiness parameter that characterizes its effects on velocity profiles and turbulence in flooded surface flows.

Takahashi [13] proposed the following parameter in order to analyze one-dimensional (1-D) hydraulic equations of flood waves.

$$\lambda \equiv \frac{V_s}{C \sin\theta} \tag{9}$$

where, $V_s \equiv (h_p - h_b)/T_d$ (10),

and $C = \sqrt{g h_p}$ (11).

T_d is the duration time from the base discharge to the peak discharge in flood. The subscripts b and p denote the " base " and " peak " values, respectively. The parameter λ implies the ratio of the rising speed V_s of water surface to the vertical component of celerity C of long waves. Nezu *et al.* [8] have used the value of λ as an unsteadiness parameter. However, its parameter may not be suitable to compare unsteady flows over smooth bed with those over rough beds, because these values of bed slope $S_b = \sin\theta$ are quite different from each other.

Therefore, Nezu *et al.* [9-12] have proposed the following new parameter α that correlates with the pressure gradient dP/dx. Using (4), one can obtain

$$\alpha \equiv \frac{1}{U_c}\frac{h_p - h_b}{T_d} = \frac{V_s}{U_c} \cong \frac{1}{\rho g}\frac{dP}{dx} \text{ for the rising stage} \tag{12},$$

$$\text{since } \frac{1}{\rho g}\frac{dP}{dx} = \left(\frac{1}{U_c} - \frac{1}{C}\right)\frac{\partial h}{\partial t} \cong \frac{1}{U_c}\frac{\partial h}{\partial t} \tag{13}.$$

U_c is the convection velocity of turbulent eddies, and is roughly equal to $(U_b + U_p)/2$. The parameter α is the ratio of the rising speed V_s of the flooded water surface to the convection velocity U_c.

It is strongly suggested [5, 14] that the pressure gradient dP/dx characterizes the properties of unsteady boundary layers in a similar mechanism to those of accelerating and decelerating flows. Clauser [15] defined a pressure-gradient parameter, as follows:

$$\beta = \frac{\delta^*}{\tau_b}\frac{dP}{dx} \tag{14}$$

δ^* is the displacement thickness. The Lausanne's group of Graf have used β or its equivalent as a parameter of accelerating/decelerating steady flows [16] and unsteady flood flows [7] in open channels. From (12) and (14), one can obtain

$$\alpha \cong \frac{U_*^2}{g\delta^*}\beta > 0 \text{ for the rising stage} \tag{15}$$

The overall unsteadiness parameter α is in proportion to the local pressure-gradient parameter β and the Froude number $Fr_* = U_*/(g\delta^*)^{1/2}$. Therefore, α implies that the adverse pressure-gradient ($\beta > 0$) appears in the rising stage of floods ($\alpha > 0$), which corresponds to the decelerating period of unsteady duct flow. Kadota [17] has recently discussed such large differences of turbulent flow between open (free surface) and closed (rigid wall) channels.

2.3 General Log-Law and Evaluation of Friction Velocity

The mean velocity U is described using the mixing-length model, as follows (e. g., see the IAHR monograph [1]):

$$\frac{dU^+}{dy^+} = \frac{2(1-\xi)}{1+\sqrt{1+4l^{+2}(1-\xi)}} \tag{16}$$

where, $\xi \equiv y/h = y^+/R_*$, $U^+ \equiv U/U_*$, and $y^+ \equiv yU_*/\nu$ is the dimensionless y-coordinate normalized by the viscous length ν/U_*. R_* is the Reynolds number based on the friction velocity U_* and the flow depth h. In the wall or inner region ($\xi < 0.2$), the mixing length l^+ is given by using the van Driest damping function due to the viscous effect.

$$l^+ = \varkappa y^+ (1 - \exp(-y^+/B)) \tag{17}$$

in which, $\varkappa$ is the von Karman constant and B is the damping factor. One can obtain the well-known law of the wall by integrating (16) and using (17):

$$U^+ = y^+ \text{ for } y^+ \ll B \tag{18}$$

$$U^+ = \frac{1}{\varkappa}\ln(y^+) + A \text{ for } B < y^+ < 0.2R_* \tag{19}$$

A is the integration constant.

Nezu and Nakagawa [1] have reviewed the previous data of $\varkappa$ and A in steady wall shear flows with nearly zero-pressure gradient $\beta \cong 0$ and concluded that the von Karman constant is universal one of $\varkappa = 0.41$ independent of mainflow properties such as open channels, pipes and boundary layers, whereas the integration constant A is not universal but weakly dependent on flow properties and flow history; in general,

A=5.0-5.5 (smooth wall) and especially A=5.3 for smooth open channels [18]. The value of B is a function of A, and is equal to 26 at A=5.3. These values are called "standard" log-law ones for steady wall shear flows with $\beta \cong 0$.

In contrast, the effects of unsteadiness on the von Karman constant $\varkappa$ and integration constant A may not necessarily by revealed as yet in unsteady wall shear flows. Binder and Kueny [19] have conducted some measurements of the periodic velocity oscillations near the wall in unsteady closed channel flow with no free surface by making use of one-component LDA system. They suggested that the dimensionless velocity distribution of $U^+(y^+)$ in the wall region might not be affected by the unsteadiness; the "standard" log-law might be applicable to even unsteady flows. The same suggestion was also given in unsteady boundary layers by Cousteix et al. [14]. Assuming a "general" log-law in which the von Karman constant is universal one of $\varkappa$=0.41 but the integration constant A may be weakly dependent on unsteady open-channel flow properties, the authors [9-11] have first evaluated the friction velocity U_* from the measured values of the velocity gradient using $\varkappa$=0.41 and veried that the evaluated values of U_* coincided reasonably with the theoretical values of $U_* \equiv \sqrt{\tau_b/\rho}$ calculated from momentum equation (8).

Unsteady flow properties in channels are expected to be analogous to these of steady boundary layers with adverse pressure gradients, i. e., $\beta > 0$, since relation (15) is satisfied. Recently, Nagano et al. [20] have successfully conducted hot-wire measurements very near the wall in turbulent boundary layers with strong adverse pressure gradients, i. e. β=0.76-4.66. They found that the von Karman constant is surely a universal one, but the values A and B decrease with β, and thus they stressed that the "standard" log-law of constant A cannot be applicable to adverse-pressure-gradient boundary layers. These experimental findings are also supported by direct numerical simulations [21, 22].

However, a function form A=fun. (β) in the "general" log-law is not available as yet and recently was disputed in several boundary-layer-type flows. For example, Sano [23] and Miyake and Nakashima [24] have suggested that the value of A did not decrease but rather increased with the pressure gradient β in diverging/converging duct flows. The turbulent structures in rising/falling flooded open-channel flows which are investigated in this study may be more analogous to those in diverging/converging duct flows than in simple adverse-pressure-gradient boundary layers.

For the present study, we examined the validity of general log-law experimentally, and the study showed that the relation of A and β is first revealed in unsteady open-channel flows.

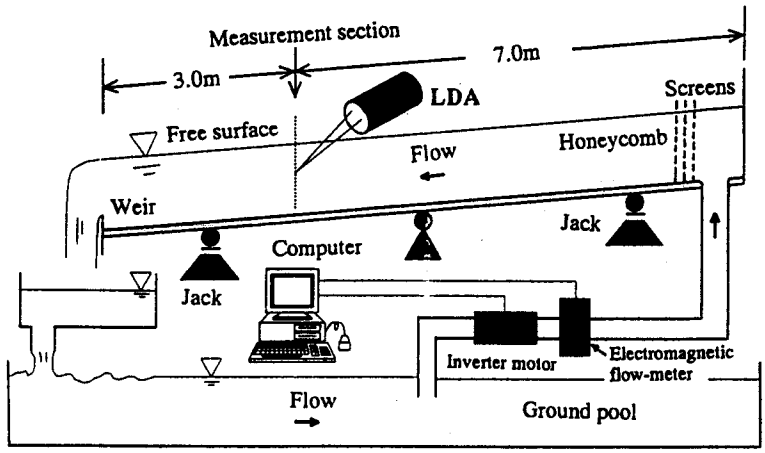

Fig. 2 Schematic description of experimental flume and water circulation system.

3. Experimental Equipment and Data Procedures

3.1 Experiments and Measurements

The experiments were conducted in a 10 m long, 40 cm wide and 50 cm deep tilting flume, as shown in Fig. 2. In this water flume, the flood discharge $Q(t)$ can be automatically controlled by a computer in which the rotation speed of a water-pump motor involving an inverted transistor is controlled by the feedback from the signals of an electromagnetic flowmeter. If any hydrograph of flood flow is input through a disc or a keyboard into the computer, the corresponding discharge can be reproduced accurately in this circulation system.

Two components of instantaneous velocities ($\tilde{u}$, $\tilde{v}$) were measured with a three-beam LDA system operated in the forward-scattering differential mode (DANTEC-made). The LDA system is especially powerful to measure velocities near the flooded free surface in unsteady open-channel flow. For example, the present LDA system can measure velocity components accurately even in the water-depth increasing region $h_b < y < h_p$ because there is no physical probe, as schematized in Fig. 1. The flow depth $h(t)$ was measured by two sets of condenser-type water-wave gauges. The slope S_s of water surface in (6) was estimated from $\Delta h/\Delta x$ using these gauges; in this study, the distance Δx between the two gauges was set to be equal to 2.0 m. All of the output signals of the LDA and gauges were recorded in digital form with a sampling frequency $f=200$-400 Hz and sample size $N=10000$-50000, depending on the hydraulic conditions. Statistical analyses were conducted then using a

large digital computer in the Data Processing Center, Kyoto University.

Seven experiments were carried out in the duration time of flood, i. e., T_d=30 s, 60 s, 90 s, and 120 s, for a smooth bed of S_b=1/600 and 10^{-4}. The base-flow depth h_b was kept constant at 4.0 cm in all cases, and the bulk mean velocities U_b of the base flow were 15.6 cm/s and 31.3 cm/s. In each case, the ratio of the peak to base discharges was changed to Q_p/Q_b=1.5, 3, 4 and 5. In these experiments, the unsteadiness parameter α varied from 0.31×10^{-3} to 2.25×10^{-3}. According to Nezu's [1] criterion of channel, the effects of secondary currents cannot appear in the center line of a channel, i. e., the test section of this study, because the aspect ratio B/h_p was larger than 5 for all cases.

3.2 Analytic Methods of Unsteady Flows

One of the most difficult aspects of the investigation of turbulent structures in unsteady flows is how to separate the mean-velocity component $U(t)$ and the turbulence component $u(t)$ from the instantaneous velocity $\tilde{u}(t)\equiv U(t)+u(t)$. Three methods to define the mean velocity are considered : (a) *the ensemble-average method*, (b) *the moving time-average method*, and (c) *the Fourier-component method*. The ensemble average method is the best one theoretically, in which the same phase of flow must be used as a trigger of sampling. This method is often used in periodic pipe flows and oscillating boundary layers, e. g., *see* the review paper written by Carr [5].

Nezu and Nakagawa [8] have examined the applicability of these three methods to unsteady open-channel flows and concluded that the Fourier-component method was the most suitable for flood surface flows because it was very difficult to determine accurately the same phase of flood waves from the wave-gauge signals. The Fourier-component method is given in the following way. Using a discrete Fourier transform (DFT), the instantaneous discrete velocity u_j (j=0, 1, 2,$\cdots$ N-1) can be transformed into a frequency domain. Only the frequency components lower than f_c =$(m-1)(2T)$ are used as representations of mean velocity U_j, as follows :

$$U_j=\frac{1}{2}a_0+\sum_{k=1}^{(m-1)/2}(a_k\cos\omega_{jk}+b_k\sin\omega_{jk}) \tag{20}$$

$$a_k=\frac{1}{N}\sum_{j=1}^{N}\tilde{u}_j\cos\omega_{jk},\ \text{and}\ b_k=\frac{1}{N}\sum_{j=1}^{N}\tilde{u}_j\sin\omega_{jk} \tag{21}$$

$$\omega_{jk}\equiv\frac{2\pi jk}{N}\quad(k=0,\ 1,\ 2,\cdots,(m-1)/2)$$

The cutoff frequency f_c of Fourier components for the mean-velocity component was reasonably chosen so as to be much smaller by an order of 10^{-3} than the bursting frequency of turbulence. The present study adopted the same size of Fourier

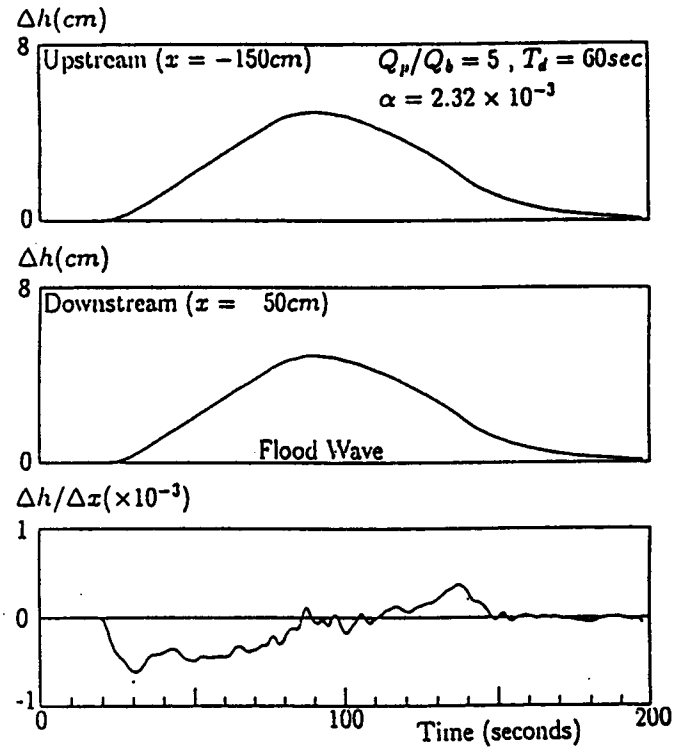

Fig. 3 Profiles of flood surface wave measured simultaneously at two points ($\Delta x = 200$ cm).

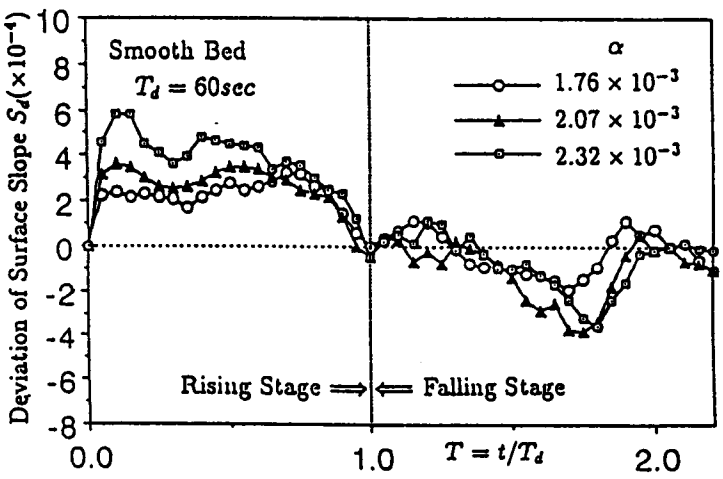

Fig. 4 Overall profiles of surface slope of flood flow against the normalized time T. The deviation from the base flow, i. e., $S_d(T) = S_s(T) - S_s$ $(T=0)$ is plotted.

components, $m=7$, for mean velocity as used in Nezu and Nakagawa [8].

4. Results and Discussion

4.1 Profiles of Flood Waves

The water-depth variation $\Delta h \equiv (h-h_b)$ measured by the water gauge, and the corresponding instantaneous velocity components ($\tilde{u}$, $\tilde{v}$) in the mainflow region ($y < h_b$) that were measured with the LDA system are shown in the authors' recent papers [9-11].

Fig. 3 shows an example of flood waves which were measured simultaneously by two sets of gauges. These were set upstream and downstream from the velocity measurement location, $x=0$. The distance between the two gauges was set at $\Delta x=$ 2 m. The surface gradient $\Delta h/\Delta x$ against the time is also plotted in Fig. 3. Although the measuring accuracy of $\Delta h/\Delta x$ might be comparatively low due to the small differences between the gauge signals, the noticeable properties were recognized in all cases of experiments. The value of $\Delta h/\Delta x$ becomes negative in the rising stage of flood, whereas it becomes positive in the falling stage. The slope of the free surface, S_s, against the horizontal axis is approximately given by $\sin\theta - \cos\theta \times \Delta h/\Delta x$, from Eq. (6).

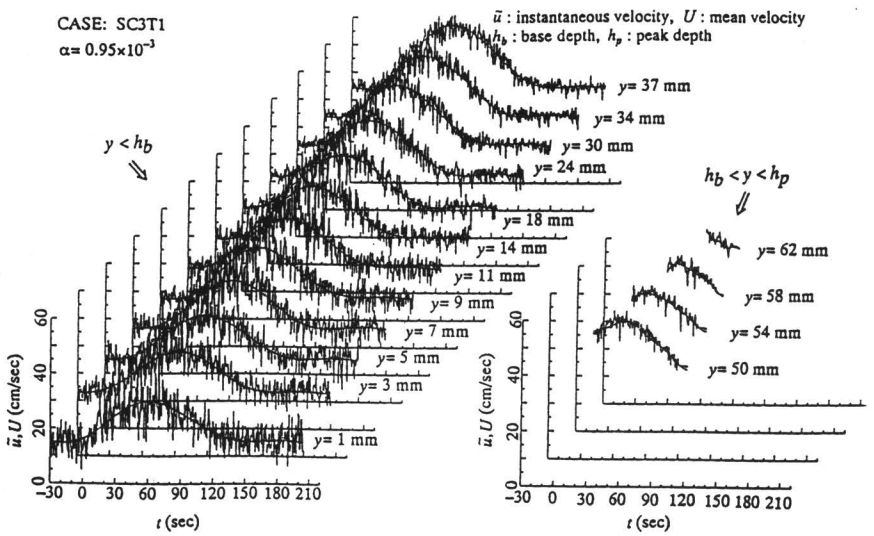

Fig. 5 Signals of instantaneous streamwise velocity in the whole flow depth including the depth-varying zone.

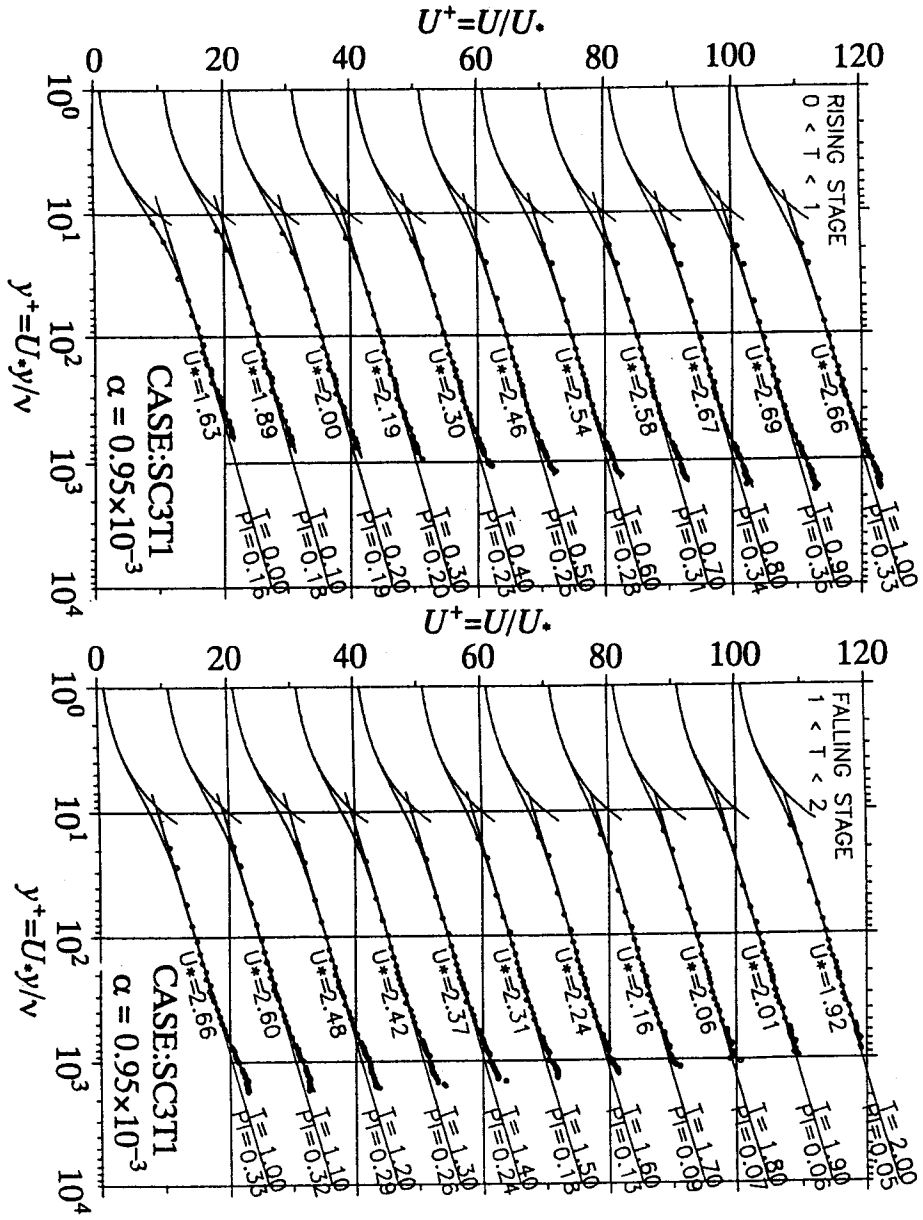

Fig. 6 Distributions of mean velocity $U^+(y^+)$ at each time $T=t/T_d$ in unsteady open-channel flows.
The friction velocity U^* and wake parameter PI=Π are indicated at every time T.

Fig 4 shows the variation of $S_d(T) \equiv S(T) - S_s(0)$ against the normalized time $T \equiv t/Td$, as a function of the unsteadiness parameter α. The value of S_d was calculated from the measured value of $\Delta h/\Delta x$. In Fig. 4, the duration time T_d is fixed at 60 seconds. $S_d(T)$ means a deviation from the water-surface slope of the base flow, i. e, $S_s(T<0)$. The value of S_d increases rapidly in the beginning of the rising stage of flood and attains maximum. Then, it decreases slowly with as increase of T. In the falling stage, the value of S_d tends to become negative, and it shows an almost anti-symmetric curve with regard to the peak-depth time, i. e., $T=1$.

These findings are very important for the consideration of the time variations of bed shear stress τ_b in unsteady open-channel flows. The property of surface gradient S_s explains why the bed shear stress τ_b becomes larger in the rising stage of flood than in the corresponding falling stage.

4.2 Profiles of Instantaneous Velocity in All Regions

Fig. 5 shows an example of the instantaneous streamwise velocity component $\tilde{u}(t)$ in all regions from the bed up to the free surface. Especially, even the water-depth increasing region $h_b < y < h_p$ could be measured accurately with the

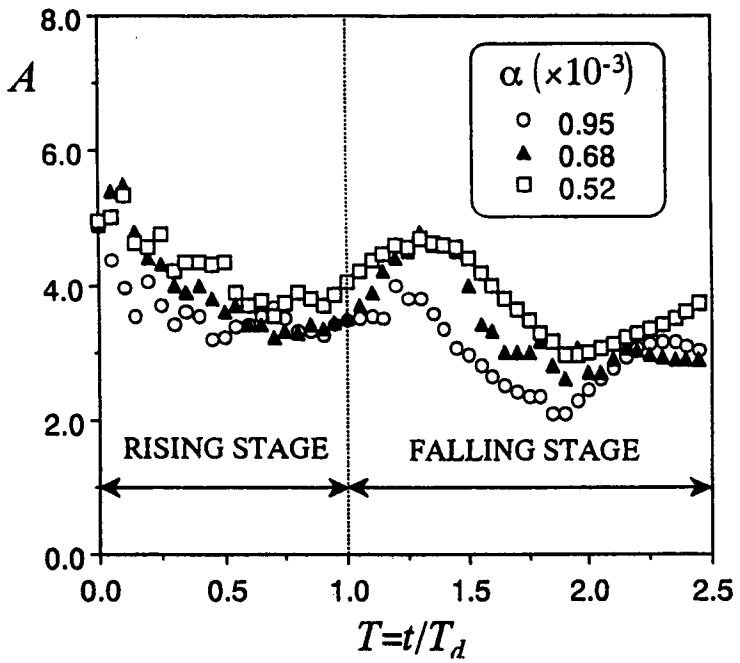

Fig. 7 Variations of integration constant A against the flood time T.

present LDA system. For comparison, the smooth curves of mean velocity $U(t)$ that were analyzed using the Fourier-component method, i. e., Eq. (20), are included in Fig. 5. The deviations from these smooth curves imply " turbulence " in this study.

4.3 General Log-Law Distribution of Mean Velocity in the Wall Region

Fig. 6 shows the distributions of mean velocity $U^+(y^+)$ as a function of normalized flood time T in the case of unsteadiness parameter $\alpha=0.95\times10^{-3}$. Almost the same results were obtained in the other cases. The figures on the left-hand side indicate the velocity profiles for the rising stage, i. e., $0<T<1$, whereas the figures on the right-hand side indicate those for the falling one, i. e., $1<T<2$. The measured values of mean velocity $U(y\,;\,T)$ in the wall region ($\xi=y/h<0.2$) except for the viscous sublayer obeyed the linear curve very well in the semi-log plot, irrespective of the rising and falling stages. Therefore, the friction velocity U_* could be evaluated from the " general " log-law (19) with the von Karman constant $\varkappa=0.41$. Fig. 6 indicates the evaluated value of U_* at each time T. The inner-variable descriptions of $U^+\equiv U/U_*$ vs. $y^+\equiv yU_*/\nu$ were plotted in Fig. 6. Each distribution is shifted by 10 units in U^+ to avoid confusion. The observed values of $U^+(y^+)$ coincide very well

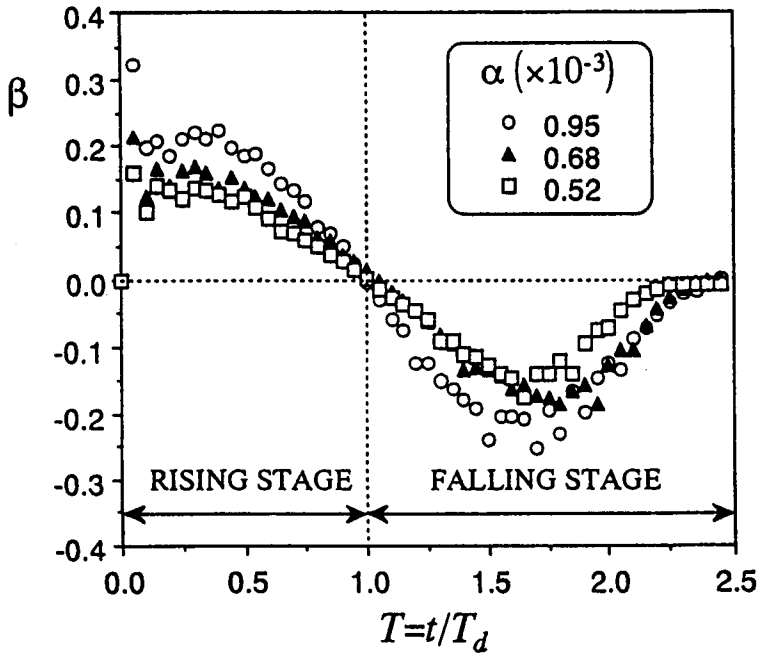

Fig. 8 Variations of Clauser's pressure-gradient parameter β against the flood time T.

with the "general" log-law (19) in the region $30<y^+<0.2\,R_*$ for every flood time.

The viscous sublayer profile of (18) and the buffer layer profile calculated from (16) and the van Driest mixing model (17) are also shown by solid curve in Fig. 6. The damping factor B in (17) was determined so that the calculated curve of (16) coincided with the general log-law distribution of (19) at $y^+=100$. The present three-beam LDA could measure velocities even at $y=0.5$ mm, which is impossible using conventional hot-film anemometers. These measured values very near the wall coincide well with the buffer-layer profile of (16), irrespective of the rising and falling stage of flood.

Fig. 7 shows the variations of the integration constant A in the log-law (19) against the normalized time T. These variations are complicated, but suggest important effects of unsteadiness peculiar to free-surface flows. The value of A at $T=0$ (base flow) coincides with that of steady open-channel flow, i. e., $A=5.3$, by Nezu and Rodi [18]. The value of A decrease with an increase of T and attains a minimum before the peak depth ($T=1$). It increases then with T and attains maximum in the middle of the falling stage. Finally, A indicates minimum at $T\approx 2$ and tends to come back to the base-flow value at $T>2$, where the flow depth h approaches the base flow.

Fig. 8 shows the variations of Clauser's pressure-gradient parameter β of (14) against time T. The value of β is positive in the rising stage, which corresponds to the adverse-pressure-gradient boundary layers. The value of A is smaller at $\beta>0$ than that of the base flow at $\beta\approx 0$, which is consistent with recent experimental results concerning the adverse-pressure-gradient boundary layer obtained by Nagano et al. [20]. It should be noted that the value of β (<0.2) for the present unsteady open-channel flow is much smaller than Nagano et al.'s values, i. e., $\beta=0.76$-4.66. This implies that the present unsteady open-channel flow corresponds to the weak adverse-pressure-gradient boundary layer.

On the other hand, β is negative in the falling stage. Although no existing experimental data of A is available at $\beta<0$, a tendency for A to increase at $\beta<0$ may be consistent with direct numerical data [21, 22]. However, a function of $A=$fun. (β) is not so simple in the falling stage of unsteady open-channel flow. This finding suggests strongly that the upstream flow history may not be neglected in the falling stage and thus affects the variation A significantly.

4.4 Log-Wake Law of Mean Velocity in the Outer Region

The values of U_* deviate from the log-law distribution of (19) in the outer region $\xi\equiv y/h>0.2$. In the same manner as steady open-channel flows [1, 18], this deviation $w(\xi)$ is described well by Coles wake function, as follows:

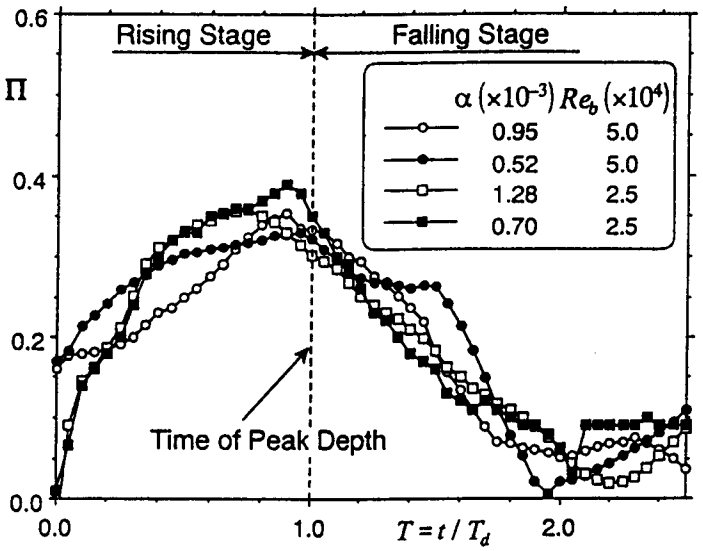

Fig. 9 Variations of wake parameter Π against the flood time T.

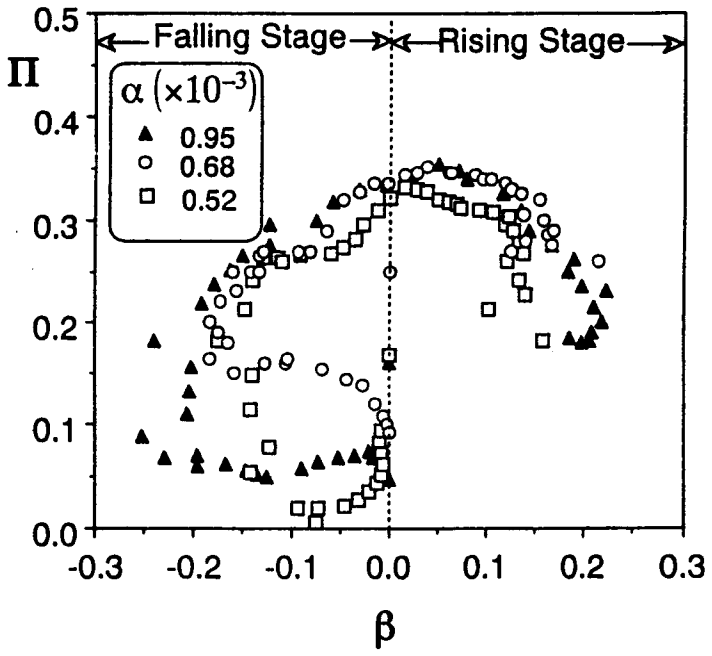

Fig. 10 Variations of wake parameter Π against the pressure-gradient parameter β.

$$U^+=\frac{1}{\chi}\ln(y^+)+A+w(\xi) \text{ for } B<y^+\leq R_* \tag{22}$$

$$w(\xi)=\frac{2\Pi}{\chi}\sin^2\left(\frac{\pi}{2}\xi\right) \tag{23}$$

The calculated curves of (22) are shown at every time T in Fig. 6. The wake parameter Π was determined by the best fitting of (23) to the observed values of U_*. Equation (22) surely describes well velocity distribution in the outer region at every time T. The Π-value is also indicated in Fig. 6.

Fig. 9 shows the variation of Π against the time T as a function of unsteadiness parameter α and the Reynolds number Re_b of base flow. Nezu and Rodi [18] pointed out that the value of Π in steady open-channel flow depends on the Reynolds number $Re=4hU_b/\nu$ of the base flow ; the Π-value increases rapidly from 0 ($Re<3\times10^4$) with an increase of Re and attains constant of 0.2 at $Re<2\times10^5$. The observed value of Π for base flow ($T=0$) was equal to zero at $Re_b=2.5\times10^4$, and it was 0.16−0.17 at $Re_b=5.0\times10^4$. These results are in good agreement with Nezu and Rodi's data [1, 18]. Still, the standard value of $\Pi=0.55$ is available in turbulent boundary layers at zero pressure-gradient, i. e., $\beta=0$. More detailed discussion is given in the IAHR-monograph [1].

Of particular significance is the noticeable difference of the Π-value in the rising and falling stages of flood ; Π indicates the strength of deviation from the log-law in the outer region including the depth-varying zone. The value of Π increases from the corresponding one of base flow with an increase of T and attains a maximum ($\Pi\cong$ 0.3-0.4) before the flow depth attains a peak h_p, i. e., $T=1$. On the other hand, it decreases with T in the falling stage and tends to come back to the base-flow value in the steady stage. Fig. 9 suggests that the overall parameter of unsteadiness, α, may not significantly affect the variations of Π vs. T.

Fig. 10 shows the variations of Π against the pressure-gradient parameter β. In this study, β also indicates the local unsteadiness of flood flow, i. e., $\partial h/\partial t$, as judged from (13) and (14). Of particular significance is the finding of counterclockwise loop of Π vs. β. The increase property of Π for the rising stage ($\beta>0$) in unsteady open-channel flow is consistent with that of the steady but adverse-gradient boundary layer ($\beta>0$). The variation of Π for the falling stage ($\beta<0$) is much more complicated than that for the rising stage ($\beta>0$). This suggests strongly that some effects of the upstream flow history may appear in the outer region for the falling stage of flood.

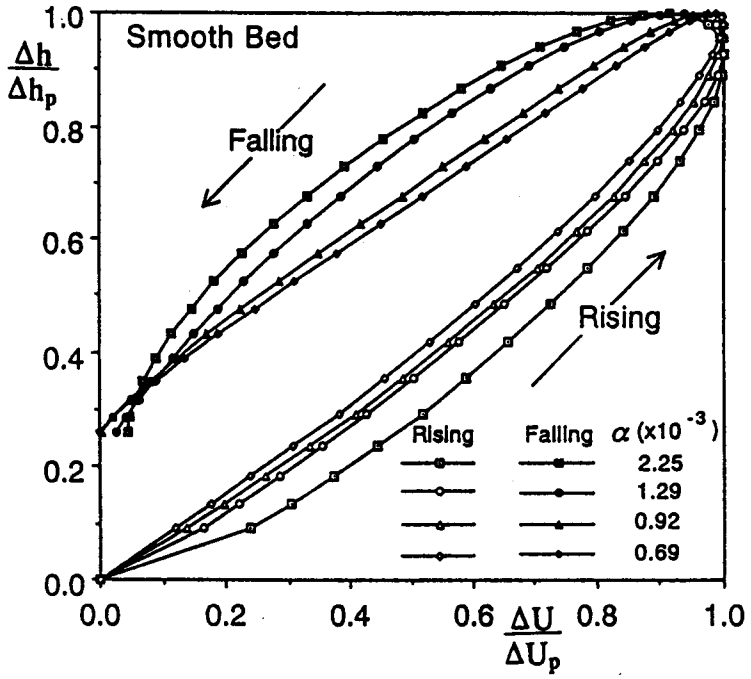

Fig. 11 Loop property of bulk mean velocity against the flow depth.

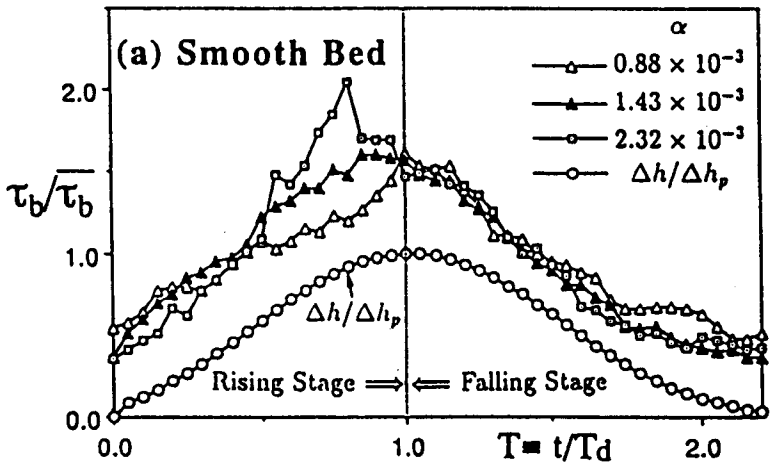

Fig. 12 Variations of bed shear stress τ_b against the flood time T.

4.5 Loop Property of Bulk Mean Velocity

The peak velocity U_p at each elevation y appeared before the flow depth h attained a peak h_p. Such a time lag between the two tended to increase closer to the bed. To examine the effect of unsteadiness on the velocity and discharge in flood, the bulk velocity $\bar{U}=1/h\int Udy$ was calculated from the measured data $U(y)$. Fig. 11 shows the curves of $\Delta U/\Delta U_p$ *vs.* $\Delta h/\Delta h_p$ as a function of α; in which, $\Delta U_p=\bar{U}-U_b$, and $\Delta h=h-h_p$. The counterclockwise loop is seen clearly in the depth-velocity diagram. As the unsteadiness of α becomes stronger, the area of the loop becomes larger. This implies that the velocity is much larger in the rising stage than in the falling one at the same flow depth for the stronger unsteady open-channel flows. These facts explain the counterclockwise loop of the depth-discharge diagram (the so-called " h-Q curve ") that is often observed in flood rivers.

4.6 Variation of Bed Shear Stress τ_b

Fig. 12 shows the variations of bed shear stress $\tau_b\equiv\rho U_*^2$ against the flood time T for a smooth bed. These values are normalized by the time-average value $\overline{\tau_b}$. U_* was evaluated from the general log-law distribution, as mentioned in 4.3. The value of $\tau_b/\overline{\tau_b}$ increases with time T and attains a maximum before the peak depth

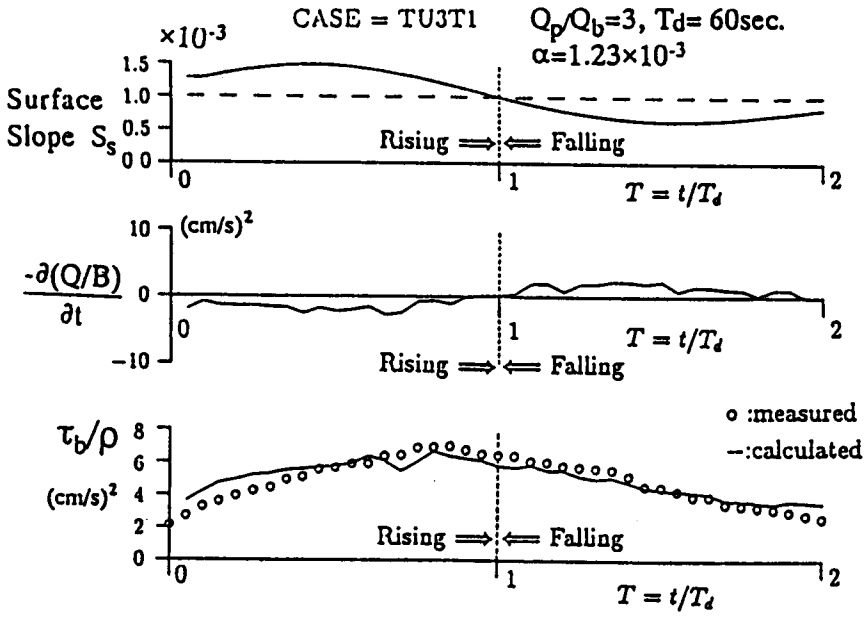

Fig. 13 Comparison between the observed values of bed shear stress τ_b and the calculated ones.

appears. On the other hand, it derceases monotonically with T in the falling stage. The maximum value of τ_b is larger and also it appears earlier before the peak depth, as the unsteadiness α is stronger. These maximum values are (3-4) times as large as the base-flow value. This suggests strongly that various sediment transports in unsteady flood flows become stronger for the rising stage than for the corresponding falling stage. These noticeable features were also recognized over rough beds in unsteady open-channel flows [10].

Fig. 13 shows a comparison between the observed values of τ_b and the calculated values from momentum equation (8). The surface slope S_s was approximated by $S_b + (1/C)\,\partial h/\partial t$, because it was less accurate to obtain $\partial h/\partial x$ from the two gauges, i. e., Fig. 4. The observed values of bed shear stress coincide well with the calculated values from the momentum equation (8). This confirms strongly the validity of the evaluation method of friction velocity U_* from the general log-law distribution even in unsteady flow. The variation of bed shear stress τ_b seen in Fig. 13 is explained mainly by the free-surface gradient S_s, and the unsteadiness of discharge $\partial Q/\partial t$ is a secondary negative contribution. These characteristics of unsteady open-channel flows are quite different from those of unsteady duct flows: in the latter case, h is constant, but S_s for the rising stage corresponds to the adverse pressure gradient $dP/dx > 0$ and thus to the decelerating flow in ducts.

4.7 Turbulence Characteristics

The turbulence intensities $u'(t)$ and $v'(t)$ were normalized by the corresponding

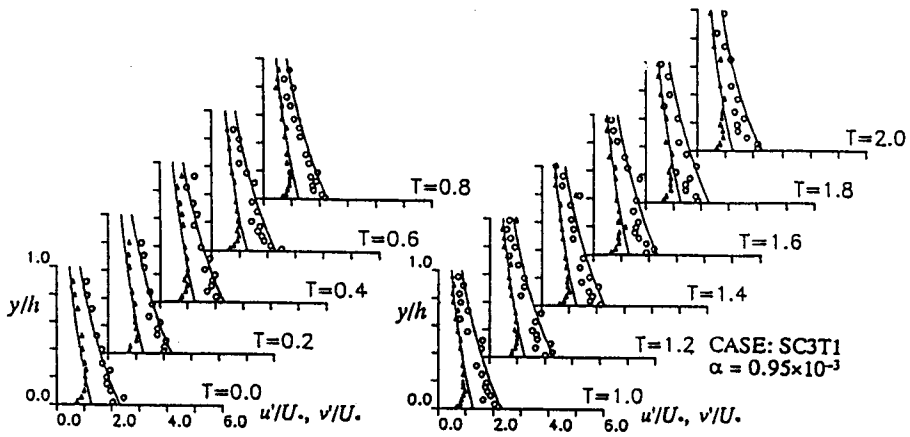

Fig. 14 Distributions of turbulence intensities u' and v' normalized by the local friction velocity U_*. The semi-theoretical curves of (24) and (25) obtained by Nezu are included.

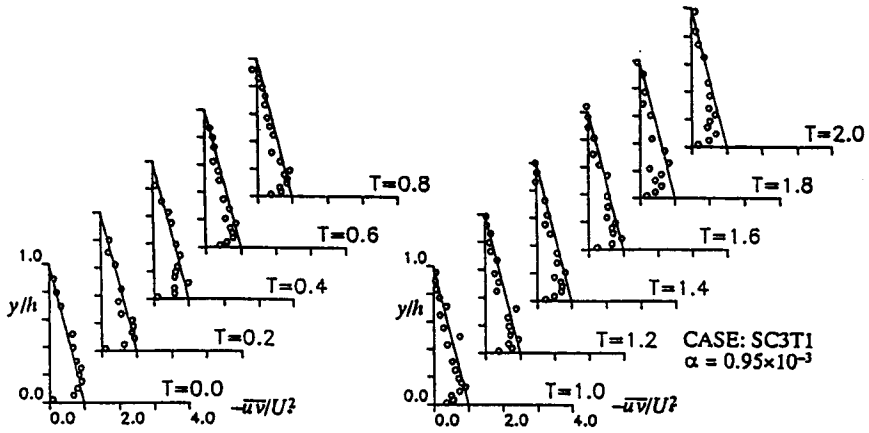

Fig. 15 Distributions of Reynolds shear stress $-\overline{uv}$ normalized by the friction velocity U_*. The theoretical curves of (7) in which the viscous term is omitted are included.

friction velocity $U_*(t)$. Fig. 14 shows an example of these results in the case of $a=0.95\times10^{-3}$. The same results were obtained for the other cases [9, 12]. In the present study however, new data near the free surface were successfully obtained and are plotted in Fig. 14. Nezu proposed the following semi-theoretical curves of turbulence intensities in steady open-channel flows, and these curves are considered to be universal functions, irrespective of Reynolds and Froude numbers; detailed discussion is given in the IAHR monograph [1].

$$\frac{u'}{U_*}=2.3\exp(-y/h) \quad (24), \text{ and } \frac{v'}{U_*}=1.27\exp(-y/h) \quad (25)$$

Fig. 14 includes the curves of (24) and (25) at each time T. The measured data of the normalized turbulence intensity u'/U_* are in good agreement with (24), although a little deviation from (24) is recognized in the falling stage. Of particular significance is that the turbulence intensity u'/U_* is not significantly affected by the unsteadiness, but coincides well with the standard data of steady wall turbulence [1]. The same results were also obtained in our earlier experiments [9]. In the same manner, the experimental values of v'/U_* in the outer region ($y/h>0.2$) coincide well with the semi-theoretical curve of (25) which is inherently valid in the intermediate region ($0.2<y/h<0.9$). v'/U_* near the wall is about 1.0 and decreases closer to the bed.

Fig. 15 shows an example of the distribution of Reynolds stress $-\overline{uv}/U_*^2$ which was measured directly with the present LDA system. Fig. 15 also includes the

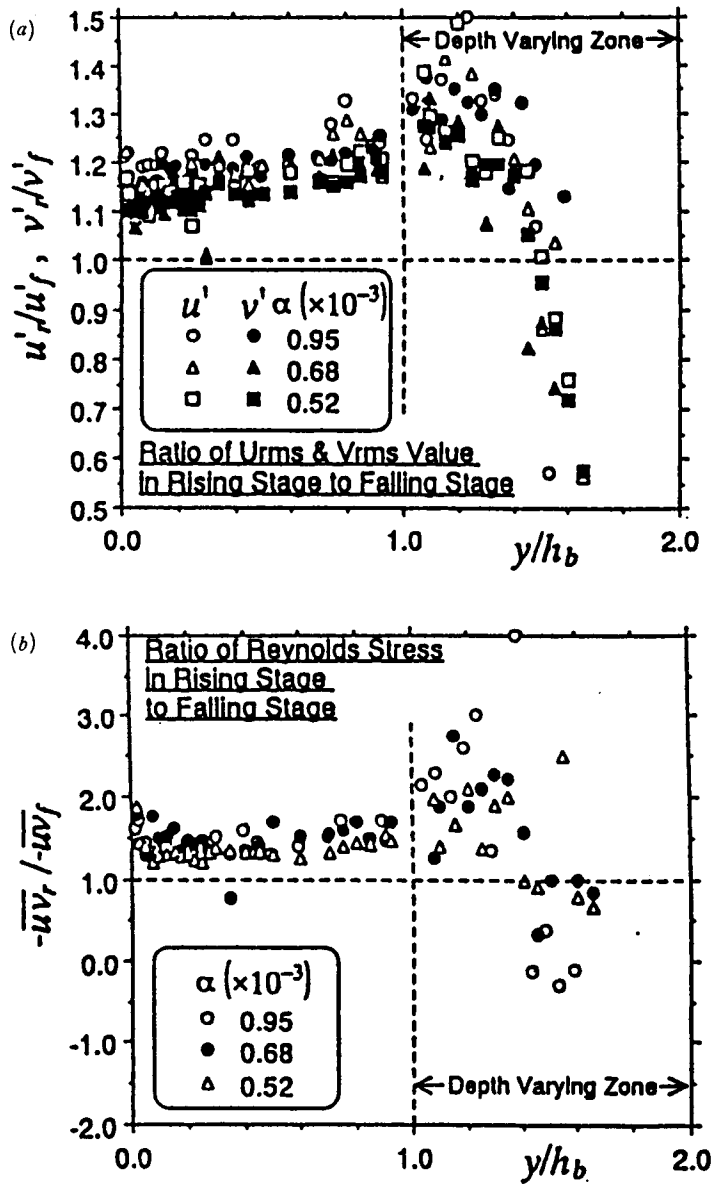

Fig. 16 The ratio turbulence of the rising flood stage to that of the falling one. (a) turbulence intensities u'_r/u'_f and v'_r/v'_f, and (b) Reynolds stress $-\overline{uv}_r/-\overline{uv}_f$.

theoretical curves of (7), in which the viscous term $\nu\partial U/\partial y$ is omitted for simplicity. The experimental values coincide well with the theoretical ones in the outer region that are approximately described by the linear distribution. This good coincidence supports again the validity of the evaluation method of friction velocity U_* from the general log-law distribution. It should be noted that the values of $-\overline{uv}/U_*^2$ even in the depth-varying zone $y>h_b=0.6\,h_p$ are in good agreement with theoretical curve, irrespective of the phase time of unsteady flood wave.

Finally, Figs. 16 (a) and (b) show the ratios of u'_r/u'_f, v'_r/v'_f and $-\overline{uv_r}/-\overline{uv_f}$. The subscript r and f denote the values averaged in the rising stage ($0<T<1$) and in the falling stage ($1<T<2$), respectively. In the base-flow zone $y<h_b$ the turbulence intensity is larger for the rising stage than for the falling one, and its ratio becomes slightly larger as the unsteadiness parameter α increases. Of particular significance is the variation of these ratios in the depth varying zone $y>h_b$. The ratio of turbulence characteristics of the rising stage to the falling stage increases with $y/h_b>1$ and attains a maximum, and then it decreases rapidly as the free surface is approached. It should be noted that the turbulence intensity very near the free surface becomes smaller for the rising stage than for the falling one, i.e., $u'_r/u'_f<1$ and $v'_r/v'_f<1$ very near the free surface. The Reynolds stress shows similar variations of the turbulence intensities.

The present noticeable data suggest that the effects of the local pressure-gradient $\partial P/\partial x$ on turbulence very near the free surface may be inverse to those on the other mainflow regions. The turbulent structure very near the free surface is not necessarily clarified as yet even in steady open-channel flows, due to the difficulties of turbulence measurements. Therefore, it is further necessary to investigate turbulence structures very near the free surface in steady and unsteady open-channel flows.

5. Conclusion

Turbulence measurements over a smooth bed in *unsteady* open-channel flows were conducted accurately by the simultaneous use of a two-component LDA system and water-wave gauges. The "general" log-law distributions in which the von Karman constant is the universal one of $\kappa=0.41$ but the integration constant A is a function of main-flow conditions were satisfied well in the wall region ($y/h<0.2$) for both the rising and falling stages of flood. The variation of A against the flood time T was first discussed. On the other hand, the log-wake law was reasonably applied to the outer region ($0.2<y/h<1.0$) including the depth-varying zone. The Coles' wake parameter Π increased for the rising stage, whereas it decreased for the falling one. The turbulence is stronger in the rising stage than in the falling one, except for

very near the free surface. The effects of unsteadiness on open-channel turbulence are condensed into the friction velocity, and consequently u'/U_*, v'/U_* and $-\overline{uv}/U_*^2$ are not so explicitly influenced by unsteadiness. Therefore, these normalized turbulence characteristics in *unsteady* open-channel flows coincide well with those in *steady* open-channel flows; the latter is discussed in detail in the IAHR monograph [1].

Of particular significance is the finding of a counterclockwise loop of the velocity and turbulence against the depth in unsteady open-channel flows. These valuable data will be contributory to the development of refined turbulence-calculation models of unsteady open-channel flows with varying free surface.

Acknowledgment

Financial support was awarded from the Asahi Glass Foundation and the Scientific Research Fund of the Government (No. 06452273), and it is herby acknowledged.

References

1) Nezu, I. and Nakagawa, H., " *Turbulence in Open-Channel Flows*," IAHR-Monograph, Balkema Publishers, Rotterdam, (1993).
2) Nezu, I., Tominaga, A. and Nakagawa, H., Field measurements of secondary currents in straight rivers, *J. Hydraulic Eng.*, ASCE, vol. 119, No. 5, (1993), pp. 598-614.
3) French, R. H., " *Open-Channel Hydraulics* ", McGraw-Hill, (1985).
4) Hasegawa, K., Simultaneous measurements of velocity and suspended sediment in Ishikari River, Report of National Government Grand-In-Aid for Scientific Research (ed. K. Ashida), (1992), pp. 45 -55, (is Japanese).
5) Carr, L. W., A review of unsteady turbulent boundary-layer experiments, *Unsteady Turbulent Shear Flows* (eds. R. Michel *et al.*), Springer-Verlag, (1981), pp. 3-34.
6) Hayashi, T., Ohashi, M. and Oshima, M., Unsteadiness and turbulence structure of a flood wave, Proc. of 20 th Symp. on turbulence, (1988), pp. 154-159, (in Japanese).
7) Tu, H. and Graf, W. H., Vertical distribution of shear stress in unsteady open-channel flow, Proc. of Inst. Civ. Engrs Wat., Marit. & Energy, vol. 96, (1992), pp. 63-69.
8) Nezu, I. and Nakagawa, H., Turbulent structures over dunes and its role on suspended sediments in steady and unsteady open-channel flows, Proc. of Int. Symp. on Transport of Suspended Sediments and Its Mathematical Modelling, IAHR, Florence, Italy (1991), pp. 165-190.
9) Nezu, I. and Nakagawa, H., Basic structure of turbulence in unsteady open-channel flows, Proc. of 9 th Symp. on Turbulent Shear Flows, Kyoto, (1993), pp. 7. 1. 1-7. 1. 6.
10) Nezu, I. Nakagawa, H., Ishida, Y. and Fujimoto, H., Effects of unsteadiness on velocity profiles over rough beds in flood surface flows, Proc. of 25 th IAHR Congress, Tokyo, Vol. A, (1993), pp. 153-160.
11) Nezu, I., Nakagawa, H., Ishida, Y. and Kadota, A., Bed shear stress in unsteady open-channel flows, Proc. of 93-Hydraulic Conference, ASCE, San Francisco, vol. 2, (1993), pp. 1458-1463.
12) Nezu, I., Kadota, A. and Nakagawa, H., Experimental study on turbulent structures in unsteady

open-channel flows, Proc. of Japan Soc. Civil Engrs., No. 491/II-27, (1994), pp. 81-88, (in Japanese).

13) Takahashi, H., Theory of one-dimensional unsteady flows in prismatic open channel, Annuals of Dis. Prev. Res., Insti., Kyoto University, vol. 12 B, (1969), pp. 515-527, (in Japanese).

14) Cousteix, J., Houdeville, R. and Javelle, J., Response of a turbulent boundary layer to a pulsation of the external flow with and without adverse pressure gradient, *Unsteady Turbulent Shear Flows* (ed. R. Michel *et al.*), Springer-Verlag, (1981), pp. 120-144.

15) Clauser, F. H., The turbulent boundary layer, Advan. Appli. Mech., vol. 4, (1956), pp. 1-51.

16) Kironoto, B. A., *Turbulence characteristics of uniform and non-uniform, rough open channel flow*, Ph. D Dissertation, Lausanne, EPFL, (1993).

17) Kadota, A., Significant difference between turbulence characteristics of unsteady flows in open channel and pipes, Proc. of 25 th IAHR Congress, Tokyo, Vol. IV, (1993), pp. 49-56.

18) Nezu, I. and Rodi, W., Open-channel flow measurements with a laser Doppler anemometer, *J. Hydraulic Eng.*, ASCE, vol. 112, (1986), pp. 335-355.

19) Binder, G. and Kueny, J. L., Measurements of the periodic velocity oscillations near the wall in unsteady turbulent channel flow, *Unsteady Turbulent Shear Flows* (ed. R. Michel *et al.*), Springer-Verlag, (1981), pp. 100-108.

20) Nagano, Y., Tagawa, M. and Tsuji, T., Effects of adverse pressure gradients on mean flows and turbulence statistics in a boundary layer, *Turbulent Shear Flows 8* (ed. F. Durst et al.), Springer-Verlag, (1993), pp. 7-21.

21) Spalart, P. R. and Leonard, A., Direct numerical simulation of equilibrium turbulent boundary layers, *Turbulent Shear Flows 5* (ed. F. Durst et al.), Springer-Verlag, (1987), pp. 234-252.

22) Spalart, P. R. and Watmuff, J. H., Experimental and numerical study of a turbulent boundary layer with pressure gradients, J. Fluid Mech., vol. 249, (1993), pp. 337-373.

23) Sano, M., Fluid flow and heat transfer in a periodically diverging-converging turbulent channel flow, Proc. of Japan Soc. Mech Engrs., vol. 58, No. 549, (1992), pp. 38-43, (in Japanese).

24) Miyake, Y. and Nakashima, M., Experimental study on wavy channel turbulent flow, Proc. of Japan Soc. Mech Engrs., vol. 60, No. 570, (1994), pp. 51-58, (in Japanese).